

Biomechanical analysis of the effect of finger joint configuration on hand grasping performance: rigid vs flexible

Yuyang Wei, Zhenmin Zou, Zhihui Qian, Lei Ren* and Guowu Wei*

Abstract — Human finger joints are conventionally simplified as rigid joints in robotic hand design and biomechanical hand modelling, due to their anatomic and morphologic complexity. However, our understanding of the effect of the finger joint configuration on the resulting hand performance is still primitive. In this study, we systematically investigate the grasping performance of the hands with the conventional rigid joints and the biomechanical flexible joints based on a computational human hand model. The measured muscle electromyography (EMG) and hand kinematic data during grasping are used as inputs for the grasping simulations. The results show that the rigid joint configuration currently used in most robotic hands leads to large reductions in hand contact force, contact pressure and contact area, compared to the flexible joint configuration. The grasping quality could be reduced up to 40% and 36% by the rigid joint configuration in terms of algebraic properties of grasping matrix and finger force limit respectively. Further investigation reveals that these reductions are caused by the weak rotational stiffness of the rigid joint configuration. This study implies that robotic/prosthetic hand performance could be improved by exploiting flexible finger joint design. Hand contact parameters and grasping performance may be underestimated by the rigid joint simplification in human hand modelling.

Index Terms - Finger joint configuration, finite element human hand model, grasping quality, finger dexterity

I. INTRODUCTION

The finger joint is made up of cartilage surfaces that connect two adjacent bones and determine the kinematics of the fingers. The complex function and anatomical structure of the interphalangeal joint have long been recognized [1-8]. Interphalangeal ligaments and joint capsules provide the stability and restraints to this flexible articulated joint. The human finger joint has been frequently imitated and simplified as a hinge joint to develop the implant [9] or robotic/prosthetic hand [10-13]. However, it is still not clear how the simplified rigid finger joints affect the hand grasping performance and whether the biomimetic flexible joint configuration can improve the robotic hand performance, although it has been found that the flexible bone-on-bone interaction restrained by the soft tissues provides sophisticated passive behavior different from the simplified

pin or hinge joint [14, 15]. There is a strong need to understand the biomechanical influences of these rigid joints on hand performance which is critical for the design of the surgical implant and robotic/prosthetic hand.

One of the typical rigid finger joint configurations is the implant introduced by Swanson [16], where the interphalangeal joint is replaced with a silastic hinge during arthroplasty. Metallic hinge-type prosthesis has been developed to replace the metacarpophalangeal or interphalangeal joint affected by the rheumatoid disease. The reliability and biocompatibility of these rigid hinge implants have been well studied [17] while their effects on hand grasping quality and dexterity after surgery have not been quantified and still remain unknown. These physical rigid finger joints have been applied in the prosthetic hand [18] and robotic hands [19, 20] to mimic the kinematics of the human finger. Torsional springs are normally used in the rigid joint to enhance the finger compliance [21, 22] or help to maintain its rest positions [23-25]. Very few of these physical hand models adopted the flexible joint containing the interphalangeal tissues. Zhe et al. [12] developed a robotic/prosthetic hand with the finger joint containing collateral ligament and volar plate. Hughes et al. [13] constructed a 3D printed soft hand skeleton with a flexible joint consisting of joint capsules and interphalangeal ligaments. However, there are no reports of whether the hand performance is improved after integrating the flexible finger joints and how the joint configurations affect the hand grasping quality. Clearly, these are the crucial pieces of information that need to be explicitly studied for designing better prosthetic robotic hands and surgical implants.

Rigid finger joint configuration has also been widely used in numerical hand models to investigate the biomechanics of finger joint and human hand contact. Very few researchers fully reconstructed the flexible phalangeal joint [26]. Hinge or universal joints are the most frequently used rigid joint to imitate finger joint kinematics. Numerical hand skeleton models with simplified hinge joints were developed to study the biomechanics of the tendon routing [27], musculotendinous force and bone-on-bone load transmission [26, 28, 29]. Anatomically intact numerical hand models were also constructed for understanding the soft contact mechanism and human tactile sensing [30, 31]. However, the effects of these simplified rigid joints on hand performance have not been considered and analyzed in these studies. Undoubtedly, the biomechanics properties of the hand skeleton, the musculotendinous force transmission and the hand contact mechanism will be influenced to some extent due to the adoption of the simplified rigid joint. Accurate representation of the human hand kinematics or

Yuyang Wei is with Department of Mechanical, Aerospace and Civil Engineering, The University of Manchester, Manchester, UK

Zhenmin Zou is with Department of Mechanical, Aerospace and Civil Engineering, The University of Manchester, Manchester, UK

Zhihui Qian is with Key Laboratory of Bionic Engineering, Ministry of Education, Jilin University, China

Lei Ren is with Department of Mechanical, Aerospace and Civil Engineering, The University of Manchester, Manchester, UK and Key Laboratory of Bionic Engineering, Ministry of Education, Jilin University, China (e-mail: lei.ren@manchester.ac.uk)

Guowu Wei is with the School of Science, Engineering and Environment, University of Salford, Salford, UK (email: G.Weil@salford.ac.uk)

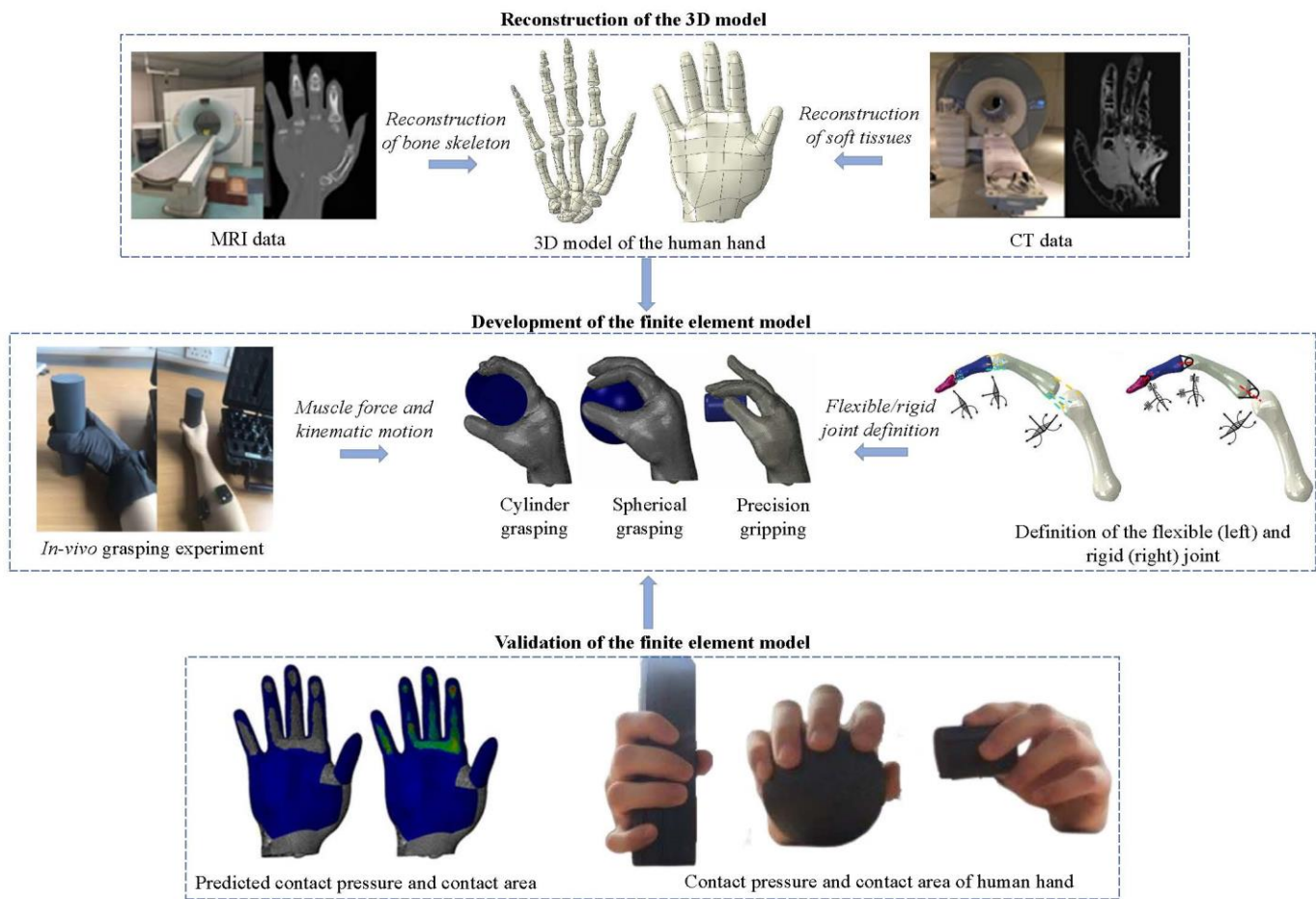


Fig.1 The main procedure of this study. From CT and MRI data processing to the development of the FE human hand model with flexible or rigid joint configuration. Simulation of three grasping postures to study the biomechanical effects of flexible and rigid finger joint configuration on hand grasping.

95 biomechanics cannot be achieved by these numerical models
96 with rigid finger joint configuration.

97 In this study, the superiority of the flexible finger joint
98 over the rigid joint is quantified by using finite element (FE)
99 human hand models with different types of joints. The rigid
100 joint is integrated with the torsional springs to simulate the
101 conventional joint configurations in robotic fingers, and the
102 resulted grasping quality is compared with that of flexible
103 joint configuration. The simulation results show that the
104 grasping quality of robotic/prosthetic hand can be improved
105 significantly by adopting the flexible finger joint
106 configuration rather than the rigid one. The computational
107 hand model with rigid joint configuration underestimates the
108 contact pressure, contact force, contact area and grasping
109 quality of the real human hand.

110 II.METHODS

111 In our previous study [30], a 23-year-old healthy male was
112 recruited and asked to sit before a table with the wrist being
113 fixed to perform the *in-vivo* grasping experiments including
114 cylindrical, spherical grasping and precision gripping. A
115 cylinder with a diameter of 50 mm and a length of 180 mm
116 was used for cylindrical grasping, a smaller cylinder with a
117 diameter of 35 mm and a length of 50 mm for precision
118 gripping. A sphere with a diameter of 80 mm was employed
119 for spherical grasping. All three objects were 3D printed with
120 Polylactic Acid and are very light. The weight of the heaviest
121 object is less than 15 grams.

122 The hand kinematics were recorded through the VICON
123 system (Virtual Motion Lab, Dallas, US) and the

124 electromyography (EMG) signals were captured by the
125 Delsys wireless EMG system (Delsys Inc., Boston, US)
126 during the *in-vivo* grasping test. The captured EMG signal
127 was filtered with a Butterworth filter (20–400 Hz) and
128 rectified. Before the grasping test, maximum voluntary
129 contraction (MVC) tests were carried out for each muscle
130 using the Jamar dynamometer and the muscle forces were
131 then computed based on the MVC forces and the processed
132 EMG signals. A linear relationship between the EMG
133 signal and muscle force for isometric muscle contracting
134 was assumed. A similar method has been used by other
135 researchers to calculate muscle forces under isometric
136 contract [32, 33]. Three main extrinsic muscles associated
137 with hand grasping and the intrinsic thenar muscles were
138 selected for measuring the muscle forces according to hand
139 anatomy and the literature [1, 34]. The subject gave
140 informed consent to participate in the grasping experiments,
141 which were approved by the Ethics Committee of the First
142 Hospital of Jilin University.

143 The CT/MR images collected from the same subject
144 were used to develop a subject-specific muscle-driven FE
145 human hand model in the commercial FE software
146 ABAQUS(Dassault Systèmes Simulia Corp, Providence,
147 RI). The FE hand model contains the intact hand skeleton,
148 subcutaneous tissue and skin, it can simulate fairly accurate
149 hand biomechanics and contact mechanism. This hand
150 model was validated against experimental data [30].

151 In the present study (See Fig. 1), this FE hand model is
152 further modified to create FE hand models with flexible
153 and rigid finger joint configurations respectively. Grasping

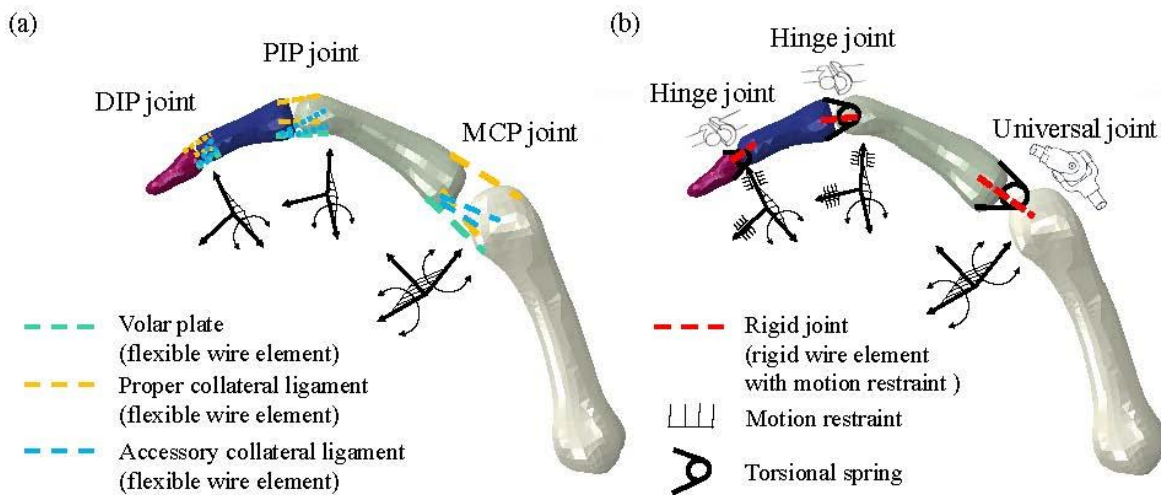


Fig. 2 The flexible and rigid finger joint configurations. (a) The collateral ligament and volar plate are simulated by using the soft wire elements. No rigid constraints are assigned to the flexible finger joints. (b) The hinge and universal joints are assigned to the phalangeal and metacarpal joints respectively. Only the rotation around a specific axis is allowed while the other degree of freedoms of the rigid joints are fixed.

Table I Relative difference between measured and predicted contact pressure

	Index		Middle		Ring		Little		Thumb	
	Flexible	Rigid	Flexible	Rigid	Flexible	Rigid	Flexible	Rigid	Flexible	Rigid
Cylindrical grasping	-5.25%	-17.25%	-9.07%	-24.29%	-6.90%	-20.86%	-9.07%	-19.76%	-3.82%	-16.15%
Spherical grasping	-5.14%	-21.64%	-7.28%	-25.74%	-3.21%	-20.22%	-5.55%	-21.23%	-5.11%	-17.23%
Precision gripping	-7.47%	-25.09%	-7.25%	-22.86%	N/A	N/A	N/A	N/A	-8.24%	-24.58%

Table II Relative difference between measured and predicted contact area

	Index		Middle		Ring		Little		Thumb	
	Flexible	Rigid	Flexible	Rigid	Flexible	Rigid	Flexible	Rigid	Flexible	Rigid
Cylindrical grasping	4.46%	-4.61%	4.50%	-5.44%	4.28%	-5.43%	3.49%	-3.54%	4.04%	-4.19%
Spherical grasping	5.47%	-5.85%	3.71%	-4.21%	4.62%	-4.77%	3.61%	-3.72%	3.89%	-4.23%
Precision gripping	4.86%	-5.02%	4.62%	-5.53%	N/A	N/A	N/A	N/A	4.17%	-4.42%

Table III Relative difference between measured and predicted contact force

	Index		Middle		Ring		Little		Thumb	
	Flexible	Rigid	Flexible	Rigid	Flexible	Rigid	Flexible	Rigid	Flexible	Rigid
Cylindrical grasping	-1.02%	-21.06%	-4.98%	-28.41%	-2.92%	-25.16%	-5.90%	-22.60%	0.07%	-19.66%
Spherical grasping	0.05%	-26.22%	-3.84%	-28.87%	1.26%	-24.03%	-2.14%	-24.16%	-1.42%	-20.73%
Precision gripping	-2.97%	-28.85%	-2.96%	-27.13%	N/A	N/A	N/A	N/A	-4.41%	-27.91%

Note: The relative differences of the magnitudes for the contact parameters between the FE hand with flexible/rigid joint and human hand are listed. The contact pressure and contact area are compared in terms of the five fingers separately, the left column stands for the differences between the FE hand with flexible finger joint and experiment measurement, while the right column represents those under rigid joint and torsional springs with the similar stiffness to those adopted in robotic hands.

154 simulations are then conducted to evaluate the grasping
155 qualities under different finger joint configurations.

156 *A. The flexible and rigid finger joints in the FE hand*
157 *model*

158 The definitions of the flexible and rigid phalangeal joints
159 are shown in Fig. 2. The flexible interphalangeal joint
160 contains the collateral ligaments on the radius/ulna side and
161 the volar plate on the palmar side (see Fig. 2a). Research has
162 shown that joint stability and kinematics are mainly restricted
163 through these two ligaments [26, 35]. The non-linear
164 wire/spring element is applied to model these interphalangeal
165 soft tissues. Such non-linear spring configurations were
166 widely used to represent the soft tissues and good simulation

167 results were achieved [36-39]. The material properties of
168 the collateral ligament and volar plate are collected from
169 the literature [40] and shown in Table S1 to S3 in the
170 supplementary material. The motion of the flexible joints
171 is assigned by using the angular displacement around the
172 rotation axis while its rotations around the other two axes
173 and the displacements along all directions are
174 unconstrained. Frictionless contact between adjacent
175 phalangeal bones is defined for all finger joints. The rigid
176 hinge and universal joints (see Fig. 2b) are used to simplify
177 the interphalangeal and metacarpophalangeal joints
178 respectively. Similar rigid joint configurations have been
179 adopted in other published computational hand models [29,
180 31, 41]. The hinge joint strictly fixes the motion of the joint

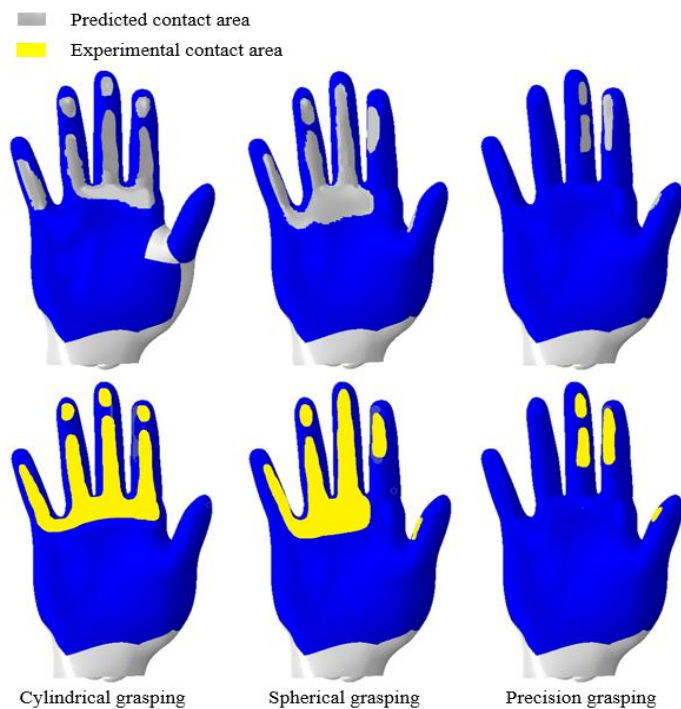


Fig. 3 Comparison of contact area between experimental measurement and FE prediction. The grey zone represents the predicted hand contact area (first row) while the yellow zone represents the measured hand contact area (second row).

181 except the flexion/extension while the universal joint only
 182 allows the flexion/extension and lateral bending. To simulate
 183 the conventional rigid joint configuration adopted in most of
 184 the existing robotic/prosthetic hands, one set of torsional
 185 springs with the stiffness of 0.027, 0.031 and 0.022 Nm/rad
 186 are configured on MCP, PIP and DIP joint respectively. The
 187 spring stiffness of 0.049 Nm/rad is used on the CMC joint.
 188 These spring stiffnesses are extracted and averaged from the
 189 literature [22, 24, 25, 42]. The grasping quality of the FE
 190 hand with rigid finger joint is compared with that of flexible
 191 joint configuration. The effect of spring stiffness on grasping
 192 performance is also investigated.

194 B. The grasping simulation and model validation

195 Cylindrical, spherical grasping and precision gripping are
 196 simulated by using the FE hand model with flexible and rigid
 197 finger joints respectively. The kinematics and muscle forces
 198 applied onto the FE hand models are from the experimental
 199 measurements in our previous study on the same human
 200 subject [30]. After the FE simulations, the normal contact
 201 force, shear contact force, contact pressure and contact area
 202 on the hand are extracted and used to assess the hand
 203 grasping quality. The typical simulation results of three
 204 grasping of the FE hand with flexible and rigid finger joints
 205 are shown in Fig. S1 in the supplementary material.

206 The FE hand model with flexible finger joint configuration
 207 is validated against the *in-vivo* grasping experimental results.
 208 The contact pressures on fingertips during the grasping
 209 experiment were detected by the pressure sensors mounted
 210 on the data glove. To measure the contact area of the human
 211 hand, red paint was daubed onto the subject's hand and a
 212 paper was wrapped onto the surface of the objects to capture
 213 the contact area of the hand. The differences between the
 214 experimental measured and FE simulated contact pressure,
 215 contact area and contact force on each finger of the hand are
 216 presented in Table I, II and III. The FE hand model with

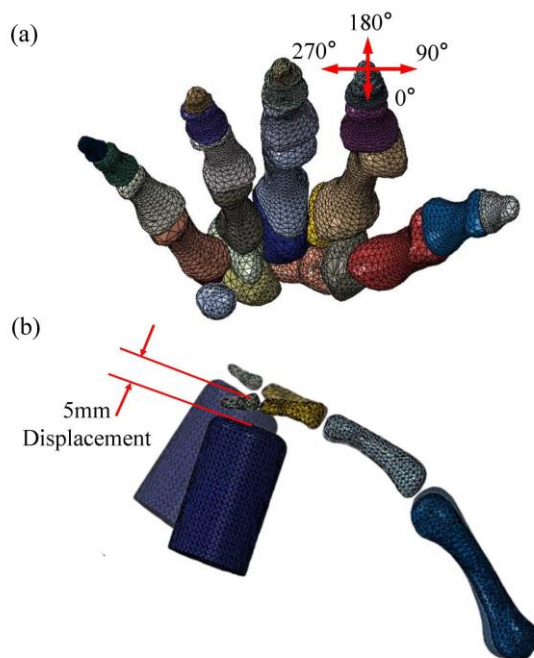


Fig.4 The simulation for calculating finger stiffness. (a) The coordinate for defining the direction of the stiffness together with the hand skeleton. (b) The simulation procedure for measuring the index finger stiffness from the direction of the angle 0°. The MCP joint is fixed while the cylinder is used to push the index finger to a displacement of 5mm.

217 flexible joint produces slightly lower contact pressures and
 218 larger contact areas than the experiment measurements, but
 219 with all the relative differences below 10%. However, the
 220 predicted contact forces are very accurate, within a 6.2%
 221 error range to the experiment forces. The detailed shapes
 222 and positions of the contact areas are displayed in Fig. 3,
 223 showing that the simulation matches well with the
 224 experimental measurement. As expected, the FE hand with
 225 rigid finger joints cannot simulate the human hand,
 226 producing much smaller contact pressures and contact
 227 forces than the experiment results.

228 The FE hand model with flexible finger joints is further
 229 validated against a grasping test of a six-axis force/torque
 230 sensor ATI Mini40 (Mini40, ATI Industrial Automation,
 231 USA) by the same subject as shown in Fig. S2 in the
 232 supplementary material. Due to the size of the six-axis
 233 force/torque sensor which is much larger than the thin-film
 234 pressure sensors, it is impractical to attach these force
 235 sensors onto the fingertip or palm for measurement during
 236 grasping. Therefore, the normal and shear contact forces in
 237 3 axial directions on the index fingertip are measured by
 238 directly gripping the force sensor. The gripping of the force
 239 sensor is then simulated using the FE human hand model
 240 with flexible joints. The predicted normal and shear contact
 241 forces on the index fingertip are in good agreement with
 242 the measured forces, with the relative differences being
 243 below 8% (See Table S4).

245 C. The evaluation of the grasping quality

246 Three types of grasping quality measures are used in this
 247 study: (1) The limits of the finger forces which is related to
 248 contact forces; (2) The geometric relations of the grasp
 249 which relate directly to the contact area (size and shape);
 250 (3) The algebraic properties of grasping matrix \mathbf{G} which
 251 depends upon contact forces and moments. The contact
 252 moments are related to both contact forces and areas.

253 Therefore, it represents the combined effect of contact areas
 254 and forces. These three types of grasping quality measures
 255 show a comprehensive assessment of the hand grasping
 256 quality which have been used by researchers [43-45].

257 From the finite element simulations of the cylinder,
 258 spherical grasping and precision gripping, the following
 259 results can be extracted as the database for the derivation of
 260 the grasping quality: (a) The contact areas on each finger. (b)
 261 The three components of the contact force, F_x , F_y and F_z , on
 262 the contact surface of the grasped object. (c) The three
 263 components of the contact moment, M_x , M_y and M_z , about
 264 the three coordinate axes on the surface of the grasped object.
 265 (d) The three contact force components, f_{xi} , f_{yi} and f_{zi} , on the
 266 surface of the i -th finger, the moment m_{zi} around axis z .

267 The external wrench \mathbf{w} on the grasped object is then
 268 obtained as $\mathbf{w} = [F_x \ F_y \ F_z \ M_x \ M_y \ M_z]^T$. The internal wrench
 269 \mathbf{f}_c is defined as $\mathbf{f}_c = [f_{x1} \ f_{y1} \ f_{z1} \ m_{z1} \ \dots \ f_{xn} \ f_{yn} \ f_{zn} \ m_{zn}]^T$.
 270 Finally, the internal wrench \mathbf{f}_c is related to the external
 271 wrench \mathbf{w} by the grasping matrix \mathbf{G} as follows [43]:

$$272 \quad -\mathbf{w} = \mathbf{G} * \mathbf{f}_c \dots \dots \dots (1)$$

273 Since \mathbf{w} and \mathbf{f}_c are already obtained from FE simulation, \mathbf{G} is
 274 determined from the above equation.

275 Based on the grasping matrix \mathbf{G} and the contact areas and
 276 forces, the following indices are employed in this study to
 277 evaluate the grasping quality.

278
 279 *Minimum singular value of G*

$$280 \quad Q_{MSV} = \sigma_{min}(\mathbf{G}) \dots \dots \dots (2)$$

281 The grasp becomes unstable when one of the singular values
 282 turns to zero and the hand will lose the capability for
 283 balancing the wrench at least in one direction. $\sigma_{min}(\mathbf{G})$
 284 indicates how far the grasp configurations is from the
 285 singular configuration [43].

286
 287 *Volume of the ellipsoid in the wrench space*

$$288 \quad Q_{VEW} = \sqrt{\det(\mathbf{G}\mathbf{G}^T)} \dots \dots \dots (3)$$

289 The grasp matrix \mathbf{G} maps a sphere of unitary radius in the
 290 force domain of the contact points into an ellipsoid of the
 291 wrench space. Q_{VEW} should be maximized to obtain the
 292 optimum grasp [43].

293
 294 *Grasp isotropy index*

295 The grasp isotropy index is defined as:

$$296 \quad Q_{GH} = \frac{\sigma_{min}(\mathbf{G})}{\sigma_{max}(\mathbf{G})} \dots \dots \dots (4)$$

297 $\sigma_{min}(\mathbf{G})$ and $\sigma_{max}(\mathbf{G})$ are the minimum and maximum
 298 singular values of \mathbf{G} . A more uniform contribution of the
 299 contact forces to the total wrench applied on the object and a
 300 more stable grasp can be achieved when the value of Q_{GH} is
 301 close to 1 [43].

302
 303 *Area of the grasp polygon Q_{AGP}*

304 A larger contact area on the object produces a more robust
 305 grasp since the grasp can resist a larger external wrench with
 306 a bigger contact area under the same contact forces [43].

307
 308 *Distance between the centroid of the contact polygon and*
 309 *the object's center of mass Q_{DCC}*

310 A shorter distance contributes to a better grasping quality
 311 [43].

312
 313 *Largest-minimum resisted wrench*

$$314 \quad Q_{LRW} = \|\mathbf{w}\| \dots \dots \dots (5)$$

315 The magnitude of the perturbation wrench that the grasp
 316 reaches under the maximum voluntary contraction forces
 317 (MVC) is defined as Q_{LRW} in this study. A larger value of
 318 Q_{LRW} means a more stable grasping [43].

319
 320 *Normal components of the forces*

$$321 \quad Q_{MNF} = \min \frac{1}{\sum_{i=1}^n f_i^2} \dots \dots \dots (6)$$

322 Q_{MNF} should be minimized to optimize the grasp [43], as
 323 larger normal components of these forces represent more
 324 efficient grasp.

325 Among the above grasping quality indices, indices Q_{MSV} ,
 326 Q_{VEW} and Q_{GH} are related to the measure of the algebraic
 327 properties of grasping matrix \mathbf{G} . Indices Q_{AGP} and Q_{DCC}
 328 are based on the geometric relations of the grasp. Indices Q_{LRW}
 329 and Q_{MNF} consider the limits of the finger forces. These
 330 grasping quality quantifying standards follow the grasp
 331 quality measures in the review paper by Roa et al. [43] and
 332 are explained in more details in [46].

333
 334 *D. The contact feasible force set and finger*
 335 *stiffness*

336 The feasible force sets (FFS) of the fingertip contact
 337 forces are computed based on the same grasping simulation
 338 but under different input of muscle forces according to
 339 Minkowski sum algorithm [47]. There are up to five muscle
 340 forces that can be applied to the fingers in the hand model,
 341 resulting in 31 combinations of these muscle forces to
 342 compute the FFS (5 individual forces, 10 different
 343 combinations of any two muscle forces, 10 different
 344 combinations of any three muscle forces, 5 different
 345 combinations of any four muscle forces and 1 for all five
 346 muscle forces). The hand contact outputs (contact forces
 347 along the three axis of the local coordinate) are computed
 348 under each of these different muscle force inputs and the
 349 convex hull of the FFS is then drawn using Minkowski sum
 350 algorithm.

351 The stiffness of the index finger and the thumb with the
 352 flexible and rigid finger joints are also determined to study
 353 the effects of the two different joint configurations. Fig. 4
 354 illustrates how the stiffness of the index finger is computed.
 355 The MCP joint is fixed, and a cylinder is used to push the
 356 finger in a specified direction to a distance of 5mm. The
 357 simulated relationship between the contact force on the
 358 fingertip and displacement of the cylinder is plotted. A line
 359 is then fitted to these data points and the slop of this line is
 360 regarded as the finger stiffness. Similar method was used
 361 by other researchers for determining the stiffness and
 362 impedance of the joint and finger [13, 48-50]. More
 363 simulation scenarios are illustrated in Fig. S3 in the
 364 supplementary material. The stiffness in different
 365 directions with and without actuating muscle forces is
 366 calculated.

367
 368 **III. RESULTS**

369 The contact pressure, contact area, normal and shear
 370 contact forces are extracted from the simulation results.
 371 The FE hand with a flexible finger joint is regarded as the
 372 baseline model. Fig. 5 presents the changes to the contact
 373 parameters and grasping qualities of the FE hand caused by
 374 the rigid joint with torsional springs similar to most of the

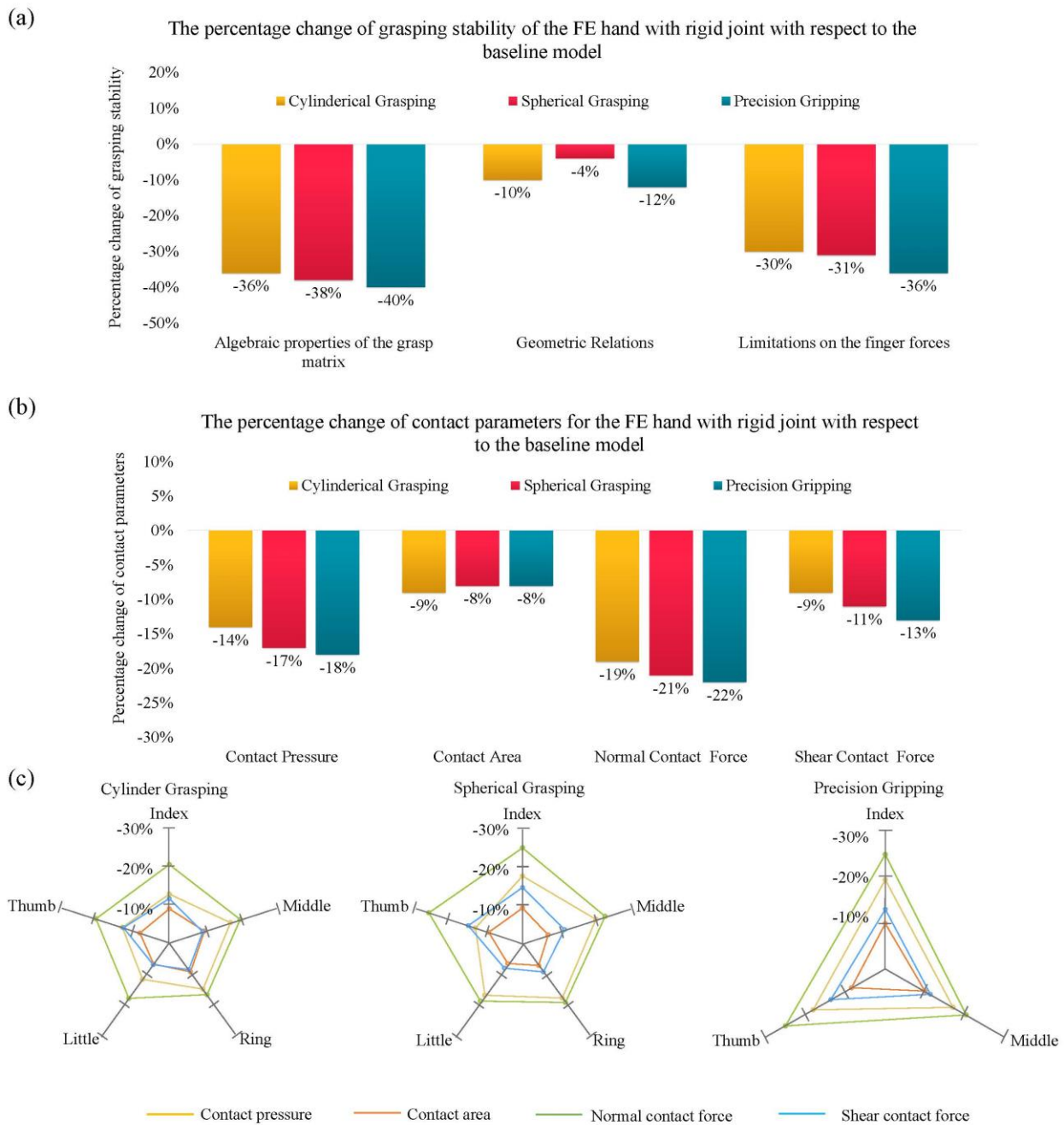


Fig.5 The percentage changes of grasping qualities and contact parameters of the FE hand with rigid joint with torsional springs similar to most of the published robotic hands with respect to the baseline model with flexible joint. (a) The changes of grasping qualities. (b) The changes of contact pressure, area and force on the hand. (c) The variations of the contact pressure, area and force on the fingertips. The grey regular pentagons and triangles are the scales of the differences.

375 published robotic hands with respect to the baseline model
 376 under cylindrical, spherical grasping and precision gripping.
 377 Reductions are found in contact pressure, contact area,
 378 contact force and grasping quality compared with the
 379 baseline model under all three grasping postures, resulting in
 380 the distorted convex hull of FFS and anisotropic joint
 381 stiffness as shown in Fig. 6 and Fig. 7 respectively under
 382 rigid finger joint configuration.

383 The use of rigid joint reduces the grasping quality by more
 384 than 36% in terms of algebraic properties of grasping matrix
 385 (see Fig. 5a). The geometry relation based grasping quality is
 386 least affected, only less than 12% of reduction. Among the
 387 three grasping postures, the precision gripping is the one
 388 most sensitive to the adoption of rigid finger joint, evidenced
 389 by the observation that the grasping quality indices are
 390 decreased more during precision gripping than the power
 391 grasping. The detailed variations of the grasping quality

392 evaluation indexes are presented in Tables S5-S7 in the
 393 supplementary material. The variations of contact pressure,
 394 contact area and contact force on the whole hand and each
 395 individual finger are shown in Fig. 5b and Fig. 5c
 396 respectively. Normal contact forces are decreased by 19%
 397 under cylindrical grasping, over 20% reductions are
 398 observed during spherical grasping and precision gripping.
 399 Significant reductions in the contact forces, pressure and
 400 area occur on the thumb, index and middle fingers during
 401 power grasping. Reductions less than 20% in the four
 402 contact parameters are found on the little and ring fingers.
 403 The fingertip contact pressure and force are affected more
 404 in precision gripping than in the power grasping, resulting
 405 in the more severe shrinking of the convex hull of FFS and
 406 then the reduction of grasping quality. The FFS for each
 407 grasping with two different joints configurations is
 408 presented in Fig. 6. Larger and more even convex hulls of

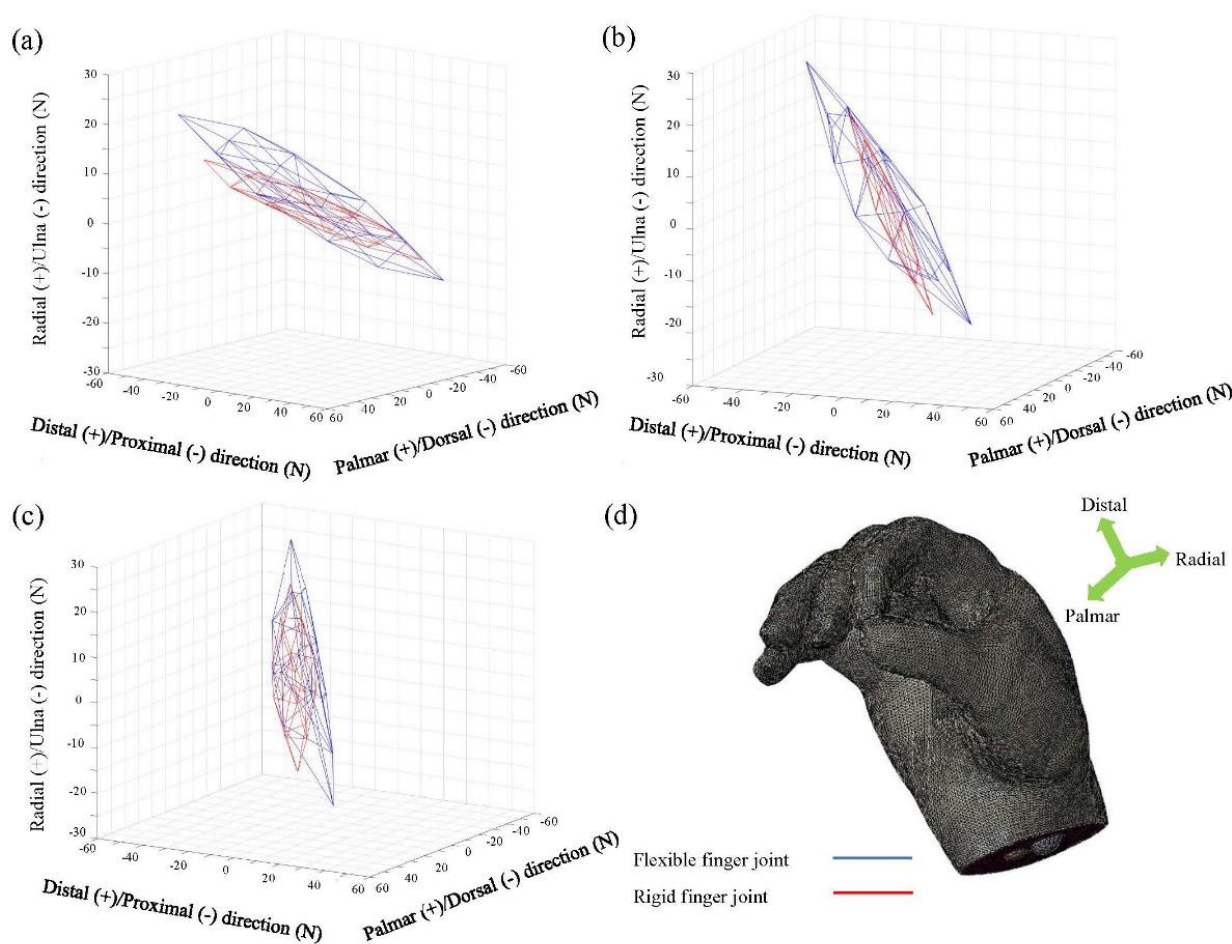


Fig. 6 Fingertip contact feasible force sets for the FE hand with rigid and flexible joints. (a) FFS for cylinder grasping. (b) FFS for spherical grasping (c) FFS for precision gripping. (d) The anatomical position defined for the FFS diagram. The volume of FFS under flexible finger joint is larger than that under rigid joint in terms of all grasping postures, indicating that a firmer grasping is achieved under flexible finger joint configuration.

409 the FFS are achieved by the FE hand with flexible joint than
 410 that of the rigid one. The reduced fingertip contact forces are
 411 responsible for the shrinking of the convex hull for the FFS
 412 of the hand with a rigid joint.

413 Fig. 7 presents the finger stiffness of the flexible joint in
 414 different directions. The stiffness distribution of the finger
 415 with rigid joint configuration and torsional springs with the
 416 stiffness of 0.027, 0.031, 0.022, 0.049 Nm/rad on MCP, PIP,
 417 DIP and CMC joint (similar spring stiffness to those adopted
 418 in robotic hand) are also presented. It can be seen that the
 419 finger with a rigid joint is much stiffer than that with flexible
 420 joint, but not in the rotation direction of the hinge and
 421 universal joints. The rigid joint increases the finger stiffness
 422 up to approximately four times larger than those of the
 423 flexible one. Similar finger stiffness variation is observed
 424 when the fingers are under the actuation of the muscles. As
 425 expected, the index finger is stiffer in radius and ulna side,
 426 while the thumb is stiffer in the ulna and palmar direction
 427 than in the other directions. The index finger and the thumb
 428 under two different finger joint configurations display
 429 anisotropic stiffness behavior. It is critical to notice that the
 430 finger with a flexible joint is much stiffer than that with the
 431 rigid joint in the motion of flexion/extension or lateral
 432 bending.

433 It is obvious that the finger stiffness under the rigid joint
 434 configurations is affected by the torsional springs. The very
 435 low stiffness of the torsional springs used in the
 436 aforementioned simulations may be the reason for the much
 437 lower finger stiffness than the human finger and contributes

438 to the undesirable hand performance of the FE hand with
 439 the rigid joint. Therefore, it is necessary to further assess
 440 the grasping quality of the rigid joint hand when the finger
 441 stiffness is comparable with the human subject. Efforts are
 442 then made to modulate the stiffness of the torsional springs
 443 in the rigid joint so that the stiffness of each finger is
 444 increased and made very close to the human finger in the
 445 direction resisting the motion of flexion. To simplify the
 446 stiffness modulation, the same spring stiffness is used on
 447 the individual rigid finger, but different spring stiffness
 448 among the different fingers. The modulated spring
 449 stiffnesses thus obtained are 0.316, 0.293, 0.237, 0.158 and
 450 0.326 Nm/rad on the joints of index, middle, ring, little and
 451 thumb respectively. These stiffnesses are at a similar level
 452 as those used/reported in the literature [51-53]. Fig.8 shows
 453 the grasping quality of the hand with the rigid joint
 454 adopting these torsional springs. It can be seen that the
 455 grasping quality is improved, but this hand is still inferior
 456 to the hand adopting flexible finger joints. There are still
 457 more than 15% reduction in the algebraic properties of
 458 grasp matrix, up to 23% shrinking with respect to the
 459 limitations on finger forces and less than 8% reduction in
 460 the geometric relation. This is because the stiffness
 461 increase of the torsional springs decreases the reductions in
 462 the contact parameters, e.g., the reduction of the contact
 463 pressure is reduced to 9%, 10% and 11% in cylindrical,
 464 spherical and precision grasping respectively, in
 465 comparison to the 14%, 17% and 18% reductions caused
 466 by the springs of lower stiffness shown in Fig. 5(b). The

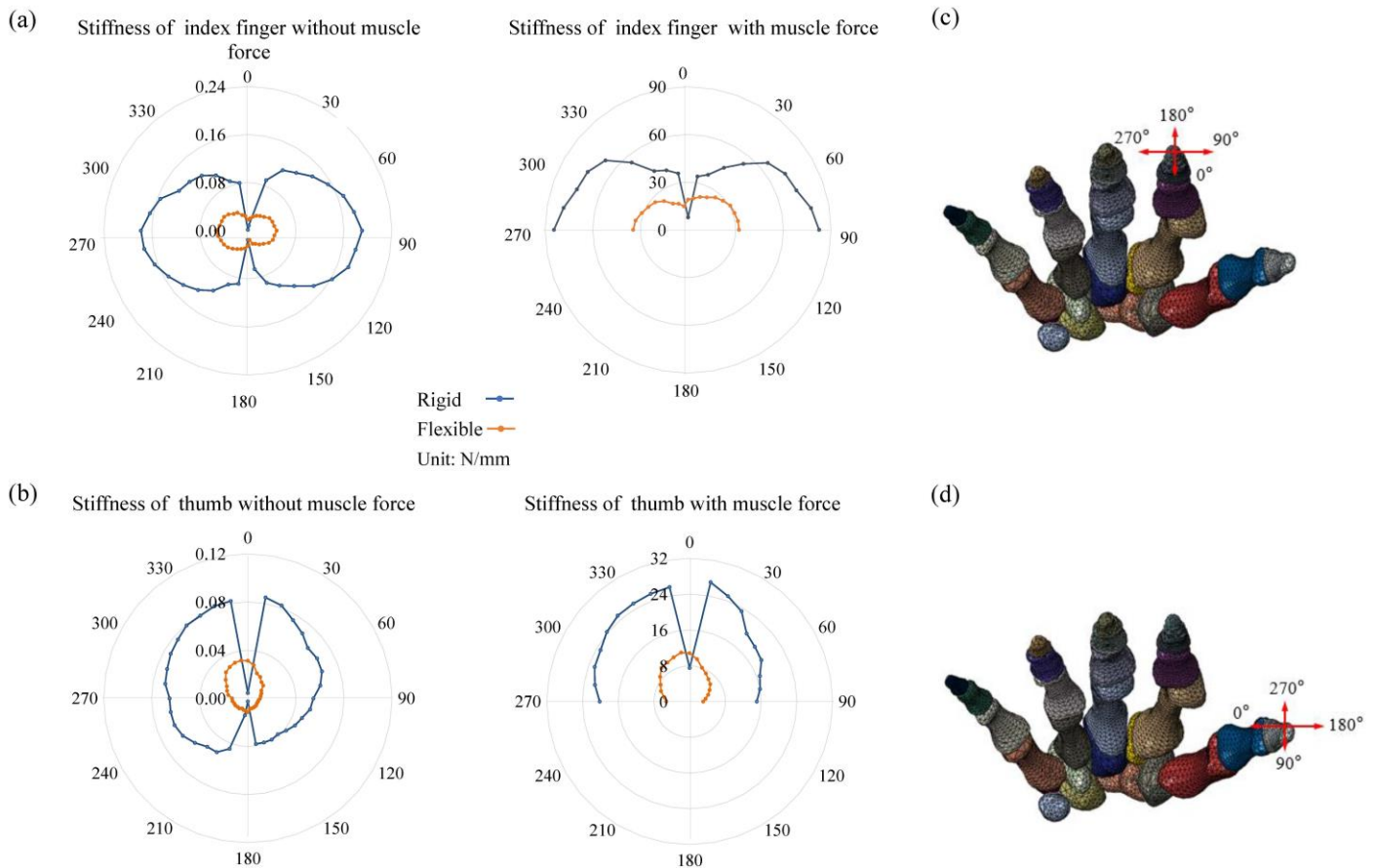


Fig. 7 The simulated stiffness (unit N/mm) of different fingers. (a). The simulated stiffness of the index finger integrating the torsional springs with similar stiffness adopted in robotic hand. The stiffness in different directions with and without actuating muscle forces are all calculated and shown in the radar plots. The finger stiffness under muscle forces is only measured from directions of palmar side or against the flexor muscle forces (0-90°, 270-360°), the stiffness toward the direction of flexor muscle forces (90-270°) are not considered in this study. The rotational direction of the torsional spring is toward to the direction of 180°. (b). The simulated stiffness of the index finger. (c). The directions for calculating the stiffness of the index finger. (d). The directions for calculating the stiffness of the thumb.

467 detailed variations of the grasping quality evaluation indexes
 468 and the stiffness distribution of the rigid finger are presented
 469 in Tables S8-S10 and in Fig. S4 in the supplementary
 470 material.

471 In summary, the numerical simulations show that the
 472 human flexible finger joint is superior to the rigid one used
 473 in robotic/prosthetic hands in all aspects, even when the
 474 stiffness of the rigid joints is increased to the similar level to
 475 the human subject.

477 IV. DISCUSSION

478 The rigid hinge and universal joints have been widely
 479 applied in robotic, biomimetic and even computational hands
 480 to represent the flexible phalangeal joint [10-12, 27, 30, 49].
 481 Some of the physical rigid joints were integrated with the
 482 torsional springs to enhance the compliance [21, 22] or help
 483 to maintain its rest position [23-25]. Whether the kinematics
 484 and biomechanical properties of the human hand can be
 485 restored through this simplified joint is still not clear. The
 486 effects of this rigid joint configuration on hand dexterity and
 487 grasping quality haven't been quantified, although these are
 488 critical information for developing finger implant,
 489 robotic/prosthetic hand and computational hand model. In
 490 this study, the superiority of the flexible finger joint over the
 491 rigid one is quantified through a FE human hand model. It is
 492 observed that flexible finger joint configuration enables
 493 larger contact parameters than the rigid joint with a lower or
 494 even similar joint stiffness, leading to a larger and even
 495 convex hull of the FFS and moderate isotropic finger

496 stiffness. All these better parameters finally contribute to a
 497 higher grasping quality.

498 The use of conventional rigid hinge/universal joint with
 499 torsional springs adopted in robotic hands reduces the hand
 500 grasping quality significantly due to its adverse effect on
 501 the contact parameters. The numerical results show that the
 502 normal contact forces are reduced by more than 19% and
 503 shear force by more than 9% after adopting the rigid finger
 504 joint with torsional springs similar to those in robotic hands.
 505 The contact pressure and contact area are decreased as well.
 506 Lower contact pressure and smaller contact area achieved
 507 by the rigid hinge finger joint configuration lead to loose
 508 and less stable contact between the hand and the object. Fig.
 509 5c presents the variation of contact force on each fingertip.
 510 Large reductions in the normal and shear contact forces are
 511 observed on index, middle and thumb fingers. The use of
 512 torsional springs in the rigid joint hand whose finger
 513 stiffness is comparable with the human subject improves
 514 the magnitudes of the contact parameters. However, the
 515 contact pressure and contact force are still more than 9%
 516 smaller than those under flexible joint configuration and
 517 the contact areas are about 5% less as shown in Fig. 8b.

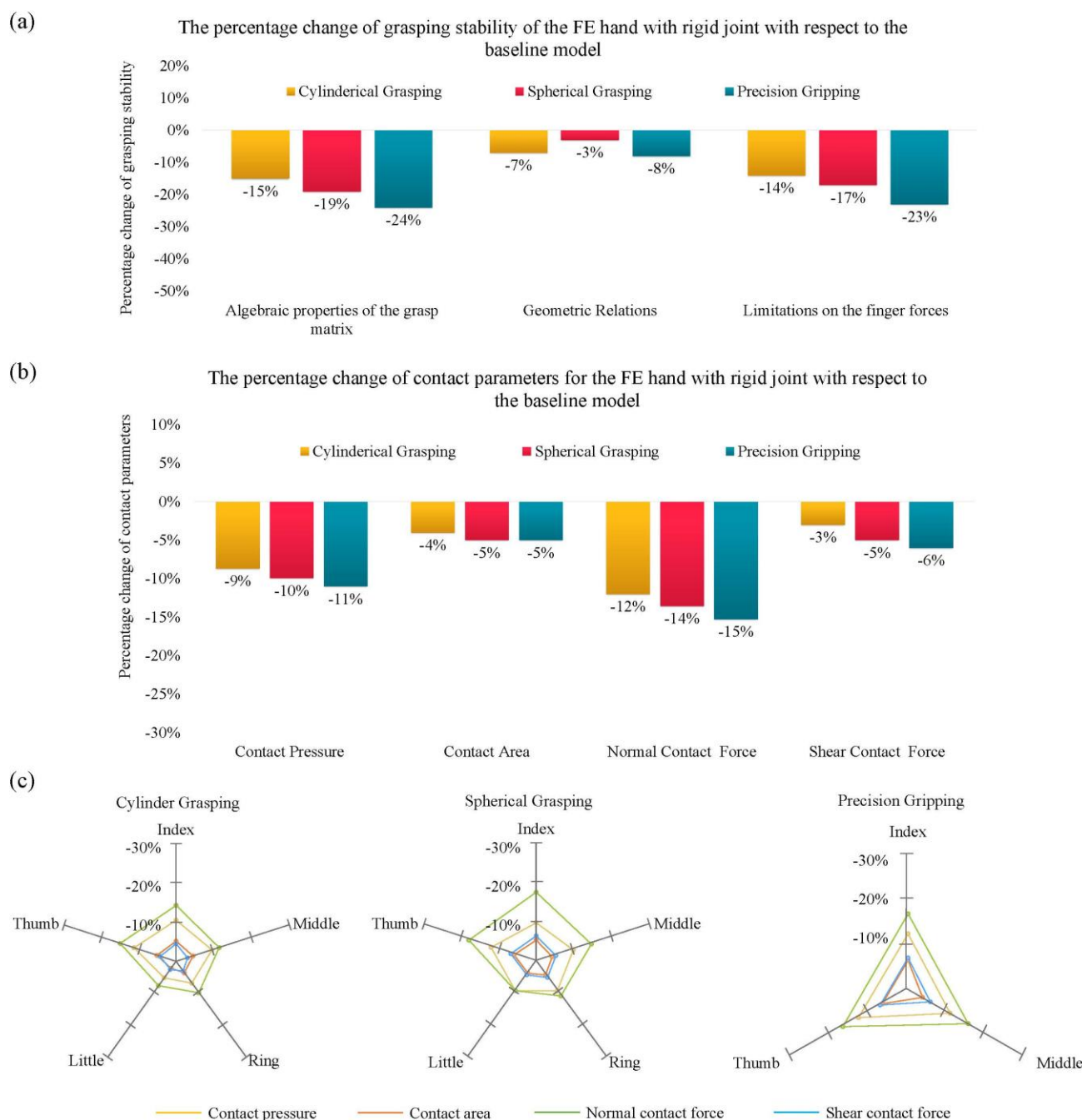


Fig. 8 The percentage changes of grasping qualities and contact parameters of the FE hand with torsional springs possessing the stiffness equivalent to human finger compared with the baseline model with flexible joint. (a) The changes of grasping qualities. (b) The changes of contact pressure, area and force on the hand. (c) The variations of the contact pressure, area and force on the fingertips. The grey regular pentagons and triangles are the scales of the differences.

518 The algebraic properties of grasping matrix and finger
 519 force limits are directly related to the contact force and
 520 contact area. Reduced contact pressure, contact area and
 521 contact force by the use of rigid joint (See Fig. 5b) lead to the
 522 distorted wrench space and then contribute to the reduced
 523 algebraic properties of grasp matrix and finger force
 524 limitations. This explains why the grasping quality
 525 associated with the algebraic properties of the grasping
 526 matrix may lose up to 40% and the finger force limits based
 527 grasping quality lose more than 30% due to the use of rigid
 528 finger joints. Fig. 5a also shows that the least affected
 529 grasping quality index is the geometry relation. This is due
 530 to the fact that geometry relation is directly associated with
 531 the contact area which is the least affected among all the
 532 contact parameters as shown in Fig. 5b. In particular, the
 533 grasping quality associated with the geometry relation is

534 reduced by only 4% during spherical grasping. This is due
 535 to the fact that the distance between the centroid of the
 536 contact polygon and the sphere's center of mass is not
 537 affected by the different joint configurations. The
 538 percentage change of Q_{DCC} (one of the sub-indices of
 539 geometric relations) is zero. On the contrary, precision
 540 gripping is very sensitive to the use of the rigid joint
 541 configuration, losing more grasping quality than the other
 542 grasping postures. This echoes the finding that significant
 543 reductions occur in contact pressure, contact area and
 544 contact forces on the three radial fingers that are involved
 545 in precision gripping as shown in Fig. 5c. This leads to a
 546 larger shrinking of the convex hull of FFS and reduction in
 547 grasping quality than power grasping where all five fingers
 548 and the palm are involved.

549 The contact force between the hand and the object is the

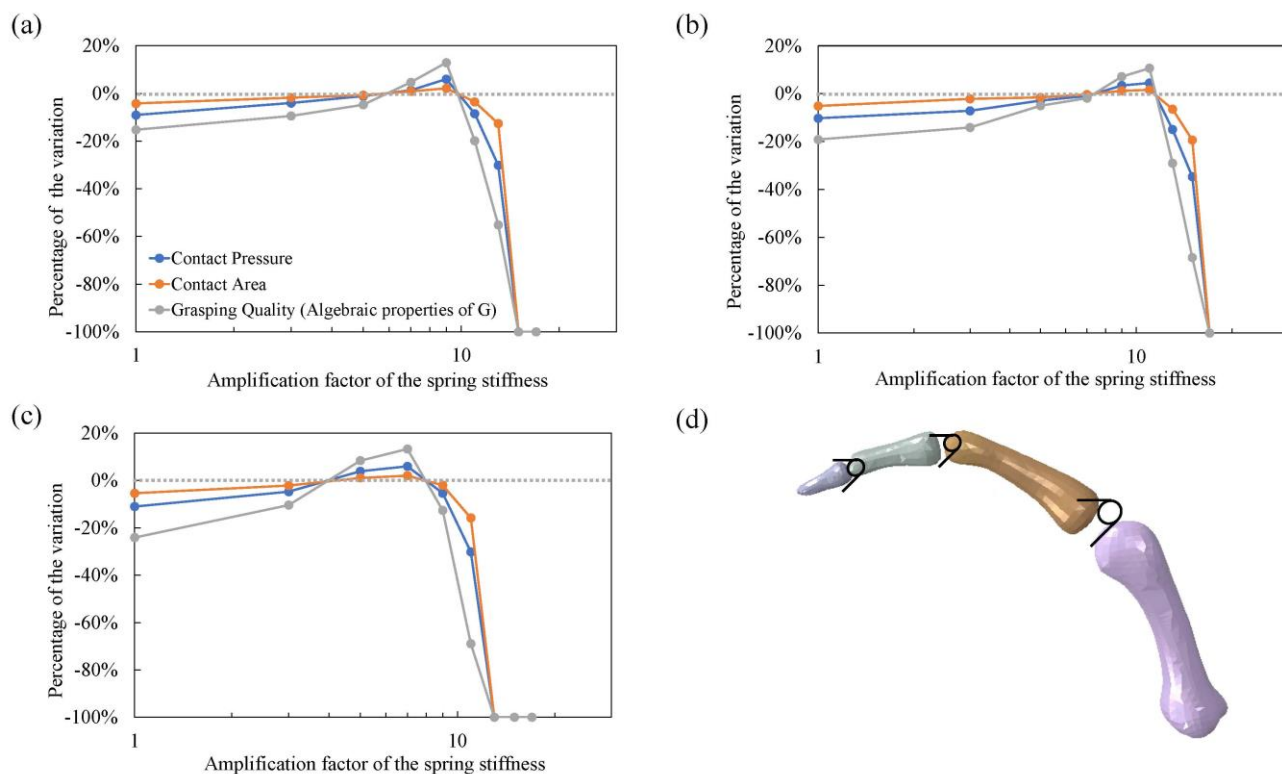


Fig. 9 The percentage changes of the contact parameters and grasping qualities of the FE hand under rigid joint configuration with torsional springs compared to that under flexible joint configuration. The torsional springs are configured at the DIP, PIP and MCP joint to enhance the stiffness of the finger and to see whether the contact pressure, contact area and grasping quality could be improved by increasing finger stiffness. The stiffnesses of the springs were multiplied from 1 to 17 (logarithmic in the diagram) based on those configured in Fig. 8 (0.316, 0.293, 0.237, 0.158 and 0.326 Nm/rad on the joints of the index, middle, ring, little and thumb). (a) Cylindrical grasping. (b) Spherical grasping. (c) Precision gripping. (d) The configuration of the torsional springs.

550 gripping force applied by the hand to the object and the
 551 reaction force from the object to the hand. During the
 552 gripping, the ability of the finger to resist the reaction force
 553 from the grasped object is the key to the grasping quality. If
 554 the finger is too flexible, then it is hard to produce a large
 555 gripping force and high grasping quality. When grasping an
 556 object, the rotation of the fingers around their joints is the
 557 main movement of the hand so that a large contact area and
 558 grasp polygon can be produced. To achieve a large grasping
 559 force, the finger should be able to resist the rotation
 560 movement caused by the contact force on it.

561 The effect of finger stiffness on grasping performance is
 562 further investigated by varying the stiffness of the torsional
 563 springs in the rigid joint based on those configured in Fig. 8.
 564 The original stiffnesses (0.316, 0.293, 0.237, 0.158 and 0.326
 565 Nm/rad on the joints of the index, middle, ring, little and
 566 thumb) were multiplied by an amplification factor ranging
 567 from 1 to 17. The obtained variations of contact pressure,
 568 contact area and grasping quality are shown in Fig. 9. As
 569 expected, increasing the stiffness of the torsional springs in
 570 the rigid joint enhances hand performance. However, to
 571 achieve a grasping quality similar to the flexible joint, a very
 572 high spring stiffness around 7 times of their original stiffness
 573 is required, much stiffer than those adopted in most of the
 574 published robotic hands [21-25]. Over-stiffened torsional
 575 spring reduces the contact pressure, contact area, and
 576 subsequently the grasping quality, echoing the finding in the
 577 literature that the robotic finger with a too large stiffness is
 578 not ideal for controlling and maintaining high dexterity on
 579 robotic or prosthetic hands [23]. A large amount of the
 580 muscles will be needed to overcome the rotation resistance
 581 of the very stiff fingers, rather than to grasp the object. When
 582 the spring stiffness approaches 17 times their initial values,

583 the muscle force cannot actuate those stiff fingers to
 584 perform the grasping at all, and the contact parameters and
 585 grasping quality are dropped to zero, resulting in a '-100%
 586 decrement' of the contact parameters as shown in Fig. 9.
 587 Therefore, optimization is needed to achieve a trade-off
 588 between the grasping quality and control difficulty when
 589 adopting torsional springs in robotic hands.

590 The rigid joint configuration with similar finger stiffness
 591 to the flexible finger joint still present grasping quality
 592 inferior to that of the flexible joint configuration. This
 593 could be explained by the fact that fingers with flexible
 594 joints possessing similar stiffness in all directions due to
 595 the combined constraints from the collateral ligaments on the
 596 radius/ulna side and the volar plate on the palmar side.
 597 On the other hand, the finger with rigid hinge and universal
 598 joints is very stiff in other directions, because these
 599 mechanical joints strictly constrain the motions of the
 600 finger except the flexion/extension and
 601 adduction/abduction. Therefore, the pronation and
 602 supination of the finger during hand grasping can hardly be
 603 performed under the rigid joint configuration while this
 604 motion is critical for maintaining precision control and
 605 hand dexterity [54, 55]. In contrast, the finger with a
 606 flexible joint has moderate and approximately isotropic
 607 stiffness. Hence, this finger with a flexible joint can move
 608 in all directions without much difficulty, enabling the hand
 609 with a higher dexterity compared with the rigid
 610 configuration with similar joint stiffness. Similar isotropic
 611 finger stiffness was reported in [13].

612 Finally, the effect of the ligament stiffness of the flexible
 613 finger joint configuration on grasping quality was also
 614 studied. The forces in the force-displacement data of the
 615 interphalangeal ligaments were multiplied by a factor

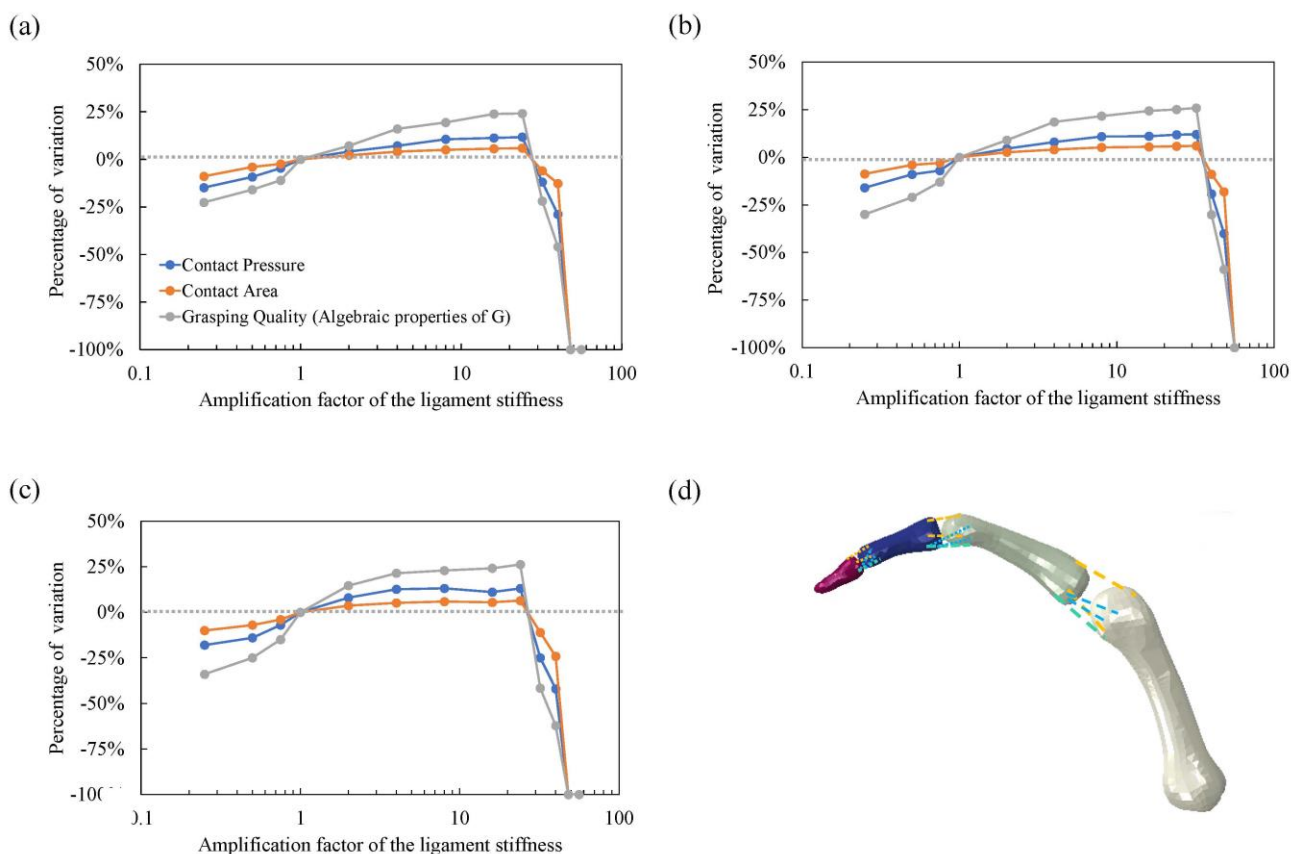


Fig. 10 The percentage changes of the contact parameters and grasping qualities of the FE hand under flexible joint configuration with modified stiffness of the ligaments. The force of the force-displacement data defining the interphalangeal ligaments was amplified by the factors ranging from 0 to 56 (logarithmic axis). (a) Cylindrical grasping. (b) Spherical grasping. (c) Precision gripping. (d) The configuration of the springs for simulating the ligaments.

616 ranging from 0.25 to 56. The resulting contact pressure,
 617 contact area and grasping quality were computed and
 618 compared with the baseline model as shown in Fig. 10. The
 619 hand performance became worse than the FE hand adopting
 620 rigid finger joint when the stiffnesses of the ligaments were
 621 reduced to 25% of their original magnitudes. The contact
 622 pressure, contact area and grasping quality increased with the
 623 hardening of ligaments, but the improving rate slowed
 624 dramatically after the amplification factor was larger than 6.
 625 The grasping quality became insensitive to the ligament
 626 stiffness in a wide range between 6 times and 24 times its
 627 original magnitudes. This enables an easy stiffness
 628 modulation for the robotic finger if adopting the flexible joint
 629 configuration. When the ligament becomes very stiff (48
 630 times their initial values), the muscle force cannot actuate
 631 those stiff finger joints, leading to a ‘-100% decrement’ of
 632 the contact parameters and grasping quality as shown in Fig.
 633 10.

634 All the results and discussions above demonstrate that the
 635 flexible finger joint is superior to the rigid one when used in
 636 the hand. The flexible joint provides the fingers with a high
 637 grasping quality but with a reasonable stiffness to resist the
 638 finger rotation. It may be crucial to have the flexible joint
 639 design in robotic/prosthetic hands by integrating flexible
 640 constraint such as artificial ligaments or capsules, so that they
 641 can restore human-like hand performance. It is believed that
 642 the use of rigid joints in the computational hand models in
 643 the literature would have underestimated the performance of
 644 the real human hand.

645 The grasping performance of the FE hand with rigid finger
 646 joints are assessed against the data from the flexible joint
 647 configuration. It would be ideal to use experimental data as

648 the benchmark for comparison if they could all be
 649 measured during the grasping tests. Unfortunately, only the
 650 contact areas and normal contact pressures can be
 651 measured by using the current technology. It is difficult to
 652 attach the force sensors onto the fingertips or palm during
 653 grasping to measure other parameters due to their large size.
 654 Therefore, it is unrealistic to obtain all the grasping quality
 655 indices through experimental measurements and use them
 656 as the benchmark for comparison. This is the reason why
 657 the finite element hand model with flexible joint is used as
 658 the benchmark model. The validation shows that the
 659 predicted contact areas and contact forces by this FE hand
 660 model both have an error of less than 6% compared to the
 661 experimental measurements. The grasping quality indices
 662 obtained from this FE hand model can represent the human
 663 hand performance with a good accuracy. Future work can
 664 focus on simulating more grasping scenarios and gain a
 665 deeper and more comprehensive understanding of the
 666 effects of finger joint configurations on hand grasping
 667 quality.

669 V. CONCLUSION

671 A subject-specific FE human hand model was employed
 672 to quantify the biomechanical effects of the rigid finger
 673 joint configuration on hand performance. The grasping
 674 quality, finger stiffness and the contact parameters
 675 including contact pressure, contact area and contact force
 676 were evaluated based on the FE hand with flexible and rigid
 677 joint configurations. It was found that the adoption of the
 678 rigid joint design with torsional springs in most of existing
 679 robotic hands reduced the contact parameters and

680 subsequently the grasping quality significantly compared to
681 the hand with flexible joint. It would be better to use flexible
682 finger joint configuration in robotic/prosthetic hands to
683 enable good grasping quality and dexterity. The results
684 indicated that more accurate contact mechanisms in the
685 human hands can only be achieved by using the flexible joint
686 rather than the rigid one based on the proposed computational
687 hand model.

689 ACKNOWLEDGEMENT

691 The authors acknowledge The University of Manchester
692 for providing the computing resources. We also want to
693 thank Dr Zhuo Wang from The First Bethune Hospital of
694 Jilin University for offering MRI and CT scanners.

696 CONFLICT OF INTEREST

698 The authors declare that they have no conflicts of
699 interest.

701 REFERENCES

702 [1] R. J. Schwarz and C. Taylor, "The anatomy and
703 mechanics of the human hand," *Artificial limbs*,
704 vol. 2, no. 2, pp. 22-35, 1955.

705 [2] W. W. Dzwierzynski, H. S. Matloub, J.-G. Yan, S.
706 Deng, J. R. Sanger, and N. J. Yousif, "Anatomy of
707 the intermetacarpal ligaments of the
708 carpometacarpal joints of the fingers," *The Journal*
709 *of hand surgery*, vol. 22, no. 5, pp. 931-934, 1997.

710 [3] N. Berme, J. Paul, and W. Purves, "A
711 biomechanical analysis of the metacarpo-
712 phalangeal joint," *Journal of Biomechanics*, vol.
713 10, no. 7, pp. 409-412, 1977.

714 [4] E. Chao, J. Opgrande, and F. Axmear, "Three-
715 dimensional force analysis of finger joints in
716 selected isometric hand functions," *Journal of*
717 *biomechanics*, vol. 9, no. 6, pp. 387-IN2, 1976.

718 [5] N. Brook, J. Mizrahi, M. Shoham, and J. Dayan,
719 "A biomechanical model of index finger
720 dynamics," *Medical engineering & physics*, vol.
721 17, no. 1, pp. 54-63, 1995.

722 [6] M. Tomaino, G. Mitsionis, J. Basitidas, R. Grewal,
723 and J. Pfaeffle, "The effect of partial excision of
724 the A2 and A4 pulleys on the biomechanics of
725 finger flexion," *The Journal of Hand Surgery:*
726 *British & European Volume*, vol. 23, no. 1, pp. 50-
727 52, 1998.

728 [7] K. D. Butz, G. Merrell, and E. A. Nauman, "A
729 biomechanical analysis of finger joint forces and
730 stresses developed during common daily
731 activities," *Computer methods in biomechanics*
732 *and biomedical engineering*, vol. 15, no. 2, pp.
733 131-140, 2012.

734 [8] I. Roloff, V. R. Schöffl, L. Vigouroux, and F.
735 Quaine, "Biomechanical model for the
736 determination of the forces acting on the finger
737 pulley system," *Journal of biomechanics*, vol. 39,
738 no. 5, pp. 915-923, 2006.

739 [9] P. Bártolo and B. Bidanda, *Bio-materials and*
740 *prototyping applications in medicine*. Springer,
741 2008.

742 [10] R. Balasubramanian and V. J. Santos, *The human*
743 *hand as an inspiration for robot hand*
744 *development*. Springer, 2014.

745 [11] J. S. Martell and G. Gini, "Robotic hands: design
746 review and proposal of new design process,"
747 *World Academy of Science, Engineering and*
748 *Technology*, vol. 26, no. 5, pp. 85-90, 2007.

749 [12] Z. Xu and E. Todorov, "Design of a highly
750 biomimetic anthropomorphic robotic hand
751 towards artificial limb regeneration," in *2016*
752 *IEEE International Conference on Robotics and*
753 *Automation (ICRA)*, 2016: IEEE, pp. 3485-3492.

754 [13] J. Hughes, P. Maiolino, and F. Iida, "An
755 anthropomorphic soft skeleton hand exploiting
756 conditional models for piano playing," *Science*
757 *Robotics*, vol. 3, no. 25, 2018.

758 [14] Y. Zhang, H. Deng, and G. Zhong, "Humanoid
759 design of mechanical fingers using a motion
760 coupling and shape-adaptive linkage
761 mechanism," *Journal of Bionic Engineering*, vol.
762 15, no. 1, pp. 94-105, 2018.

763 [15] D. Burke, S. Gandevia, and G. Macefield,
764 "Responses to passive movement of receptors in
765 joint, skin and muscle of the human hand," *The*
766 *Journal of physiology*, vol. 402, no. 1, pp. 347-
767 361, 1988.

768 [16] A. B. Swanson, "Flexible implant arthroplasty
769 for arthritic finger joints: rationale, technique,
770 and results of treatment," *JBJS*, vol. 54, no. 3, pp.
771 435-544, 1972.

772 [17] D. E. Foliart, "Swanson silicone finger joint
773 implants: a review of the literature regarding
774 long-term complications," *The Journal of hand*
775 *surgery*, vol. 20, no. 3, pp. 445-449, 1995.

776 [18] P. Slade, A. Akhtar, M. Nguyen, and T. Bretl,
777 "Tact: Design and performance of an open-
778 source, affordable, myoelectric prosthetic hand,"
779 in *2015 IEEE International Conference on*
780 *Robotics and Automation (ICRA)*, 2015: IEEE,
781 pp. 6451-6456.

782 [19] F. Rothling, R. Haschke, J. J. Steil, and H.
783 Ritter, "Platform portable anthropomorphic
784 grasping with the bielefeld 20-DOF shadow and
785 9-DOF TUM hand," in *2007 IEEE/RSJ*
786 *International Conference on Intelligent Robots*
787 *and Systems*, 2007: IEEE, pp. 2951-2956.

788 [20] C. Melchiorri, G. Palli, G. Berselli, and G.
789 Vassura, "Development of the ub hand iv:
790 Overview of design solutions and enabling
791 technologies," *IEEE Robotics & Automation*
792 *Magazine*, vol. 20, no. 3, pp. 72-81, 2013.

793 [21] D. Chakarov, M. Tsveov, I. Veneva, and P.
794 Mitrouchev, "Adjustable compliance joint with
795 torsion spring for human centred robots,"
796 *International Journal of Advanced Robotic*
797 *Systems*, vol. 12, no. 12, p. 180, 2015.

798 [22] H. Yang *et al.*, "A low-cost linkage-spring-
799 tendon-integrated compliant anthropomorphic
800 robotic hand: MCR-Hand III," *Mechanism and*
801 *Machine Theory*, vol. 158, p. 104210, 2021.

802 [23] G. P. Kontoudis, M. Liarokapis, K. G.
803 Vamvoudakis, and T. Furukawa, "An adaptive
804 actuation mechanism for anthropomorphic robot
805

806 hands," *Frontiers in Robotics and AI*, vol. 6, p. 47, 869
 807 2019. 870
 808 [24] T. E. Wiste, S. A. Dalley, H. Atakan Varol, and M. 871
 809 Goldfarb, "Design of a multigrasp transradial 872
 810 prosthesis," *Journal of medical devices*, vol. 5, no. 873 [38]
 811 3, 2011. 874
 812 [25] G. P. Kontoudis, M. Liarokapis, and K. G. 875
 813 Vamvoudakis, "A compliant, underactuated finger 876
 814 for anthropomorphic hands," in *2019 IEEE 16th 877
 815 International Conference on Rehabilitation 878 [39]
 816 Robotics (ICORR)*, 2019: IEEE, pp. 682-688. 879
 817 [26] B. Faudot, J.-L. Milan, B. Goisard de Monsabert, 880
 818 T. Le Corroller, and L. Vigouroux, "Estimation of 881
 819 joint contact pressure in the index finger using a 882
 820 hybrid finite element musculoskeletal approach," 883
 821 *Computer Methods in Biomechanics and 884 [40]
 822 Biomedical Engineering*, vol. 23, no. 15, pp. 1225- 885
 823 1235, 2020. 886
 824 [27] D. Hu, D. Howard, and L. Ren, "Biomechanical 887
 825 analysis of the human finger extensor mechanism 888 [41]
 826 during isometric pressing," *PloS one*, vol. 9, no. 4, 889
 827 p. e94533, 2014. 890
 828 [28] K. D. Butz, G. Merrell, and E. A. Nauman, "A 891
 829 three-dimensional finite element analysis of finger 892
 830 joint stresses in the MCP joint while performing 893 [42]
 831 common tasks," *Hand*, vol. 7, no. 3, pp. 341-345, 894
 832 2012. 895
 833 [29] H. I. Relf, C. G. Barberio, and D. M. Espino, "A 896
 834 Finite Element Model for Trigger Finger," 897
 835 *Prosthesis*, vol. 2, no. 3, pp. 168-184, 2020. 898
 836 [30] Y. Wei, Z. Zou, G. Wei, L. Ren, and Z. Qian, 899 [43]
 837 "Subject-specific finite element modelling of the 900
 838 human hand complex: muscle-driven simulations 901
 839 and experimental validation," *Annals of 902
 840 Biomedical Engineering*, pp. 1-15, 2019. 903 [44]
 841 [31] G. Harih, R. Nohara, and M. Tada, "Finite Element 904
 842 Digital Human Hand Model-Case Study of 905
 843 Grasping a Cylindrical Handle," *Journal of 906
 844 Ergonomics*, vol. 07, no. 02, 2017, doi: 907
 845 10.4172/2165-7556.1000190. 908 [45]
 846 [32] C. J. De Luca, L. D. Gilmore, M. Kuznetsov, and 909
 847 S. H. Roy, "Filtering the surface EMG signal: 910
 848 Movement artifact and baseline noise 911
 849 contamination," *J Biomech*, vol. 43, no. 8, pp. 912 [46]
 850 1573-9, May 28 2010, doi: 913
 851 10.1016/j.jbiomech.2010.01.027. 914
 852 [33] F. D. Farfan, J. C. Politti, and C. J. Felice, 915
 853 "Evaluation of EMG processing techniques using 916
 854 Information Theory," *Biomed Eng Online*, vol. 9, 917
 855 p. 72, Nov 12 2010, doi: 10.1186/1475-925X-9-72. 918 [47]
 856 [34] F. H. Netter, *Atlas of Human Anatomy E-Book*. 919
 857 Elsevier Health Sciences, 2017. 920
 858 [35] S. Glickel and O. Barron, "Proximal 921
 859 interphalangeal joint fracture dislocations," *Hand 922
 860 clinics*, vol. 16, no. 3, pp. 333-344, 2000. 923 [48]
 861 [36] S. D. Carrigan, R. A. Whiteside, D. R. Pichora, 924
 862 and C. F. Small, "Development of a three- 925
 863 dimensional finite element model for carpal load 926
 864 transmission in a static neutral posture," *Annals of 927 [49]
 865 biomedical engineering*, vol. 31, no. 6, pp. 718- 928
 866 725, 2003. 929
 867 [37] C. Cifuentes-De la Portilla, C. Pasapula, R. 930
 868 Larrainzar-Garijo, and J. Bayod, "Finite element 931
 analysis of secondary effect of midfoot fusions
 on the spring ligament in the management of
 adult acquired flatfoot," *Clinical Biomechanics*,
 vol. 76, p. 105018, 2020.
 M. Adouni and A. Shirazi-Adl, "Partitioning of
 knee joint internal forces in gait is dictated by the
 knee adduction angle and not by the knee
 adduction moment," *Journal of biomechanics*,
 vol. 47, no. 7, pp. 1696-1703, 2014.
 P. Tanska, M. E. Mononen, and R. K. Korhonen,
 "A multi-scale finite element model for
 investigation of chondrocyte mechanics in
 normal and medial meniscectomy human knee
 joint during walking," *Journal of biomechanics*,
 vol. 48, no. 8, pp. 1397-1406, 2015.
 G.-T. Lin, W. Cooney, P. Amadio, and K.-N. An,
 "Mechanical properties of human pulleys,"
Journal of Hand Surgery, vol. 15, no. 4, pp. 429-
 434, 1990.
 D. Chamoret, M. Bodo, and S. Roth, "A first step
 in finite-element simulation of a grasping task,"
Computer Assisted Surgery, vol. 21, no. sup1,
 pp. 22-29, 2016, doi:
 10.1080/24699322.2016.1240294.
 L. Zollo, S. Roccella, E. Guglielmelli, M. C.
 Carrozza, and P. Dario, "Biomechatronic design
 and control of an anthropomorphic artificial hand
 for prosthetic and robotic applications,"
IEEE/ASME Transactions On Mechatronics, vol.
 12, no. 4, pp. 418-429, 2007.
 M. A. Roa and R. Suárez, "Grasp quality
 measures: review and performance,"
Autonomous robots, vol. 38, no. 1, pp. 65-88,
 2015.
 B. León, J. L. Sancho-Bru, N. J. Jarque-Bou, A.
 Morales, and M. A. Roa, "Evaluation of human
 prehension using grasp quality measures,"
*International Journal of Advanced Robotic
 Systems*, vol. 9, no. 4, p. 112, 2012.
 C. Rubert, B. León, A. Morales, and J. Sancho-
 Bru, "Characterisation of grasp quality metrics,"
Journal of Intelligent & Robotic Systems, vol. 89,
 no. 3, pp. 319-342, 2018.
 Y. Wei, Z. Zou, Z. Qian, L. Ren, and G. Wei,
 "Biomechanical analysis of the effect of the
 finger extensor mechanism on hand grasping
 performance," *IEEE Transactions on Neural
 Systems and Rehabilitation Engineering*, vol. 30,
 pp. 360-368, 2022.
 M. Ciocarlie, A. Miller, and P. Allen, "Grasp
 analysis using deformable fingers," in *2005
 IEEE/RSJ International Conference on
 Intelligent Robots and Systems*, 2005: IEEE, pp.
 4122-4128.
 C. Noël, "A three-dimensional visco-hyperelastic
 FE model for simulating the mechanical dynamic
 response of preloaded phalanges," *Medical
 engineering & physics*, vol. 61, pp. 41-50, 2018.
 Q. Bi, C.-J. Yang, X.-L. Deng, and J.-C. Fan,
 "Human finger mechanical impedance modeling:
 Using multiplicative uncertain model,"
*Proceedings of the Institution of Mechanical
 Engineers, Part C: Journal of Mechanical*

- 932 *Engineering Science*, vol. 230, no. 12, pp. 1978-
933 1986, 2016.
- 934 [50] J. Z. Wu, R. G. Dong, T. W. McDowell, and D. E.
935 Welcome, "Modeling the finger joint moments in a
936 hand at the maximal isometric grip: the effects of
937 friction," *Medical engineering & physics*, vol. 31,
938 no. 10, pp. 1214-1218, 2009.
- 939 [51] D. L. Jindrich, A. D. Balakrishnan, and J. T.
940 Dennerlein, "Finger joint impedance during
941 tapping on a computer keyswitch," *Journal of*
942 *Biomechanics*, vol. 37, no. 10, pp. 1589-1596,
943 2004.
- 944 [52] D. G. Kamper, T. G. Hornby, and W. Z. Rymer,
945 "Extrinsic flexor muscles generate concurrent
946 flexion of all three finger joints," *Journal of*
947 *biomechanics*, vol. 35, no. 12, pp. 1581-1589,
948 2002.
- 949 [53] P.-H. Kuo and A. D. Deshpande, "Muscle-tendon
950 units provide limited contributions to the passive
951 stiffness of the index finger metacarpophalangeal
952 joint," *Journal of biomechanics*, vol. 45, no. 15,
953 pp. 2531-2538, 2012.
- 954 [54] W. N. Timm, S. W. O'Driscoll, M. E. Johnson, and
955 K.-N. An, "Functional comparison of pronation
956 and supination strengths," *Journal of hand therapy*,
957 vol. 6, no. 3, pp. 190-193, 1993.
- 958 [55] W. Zhang, V. M. Zatsiorsky, and M. L. Latash,
959 "Finger synergies during multi-finger cyclic
960 production of moment of force," *Experimental*
961 *brain research*, vol. 177, no. 2, pp. 243-254, 2007.
962